



Temporal Evolution of the Rotation of the Interplanetary Magnetic Field B_x , B_y , and B_z Components

N. B. Xiang^{1,2,5}, Z. J. Ning² , and F. Y. Li^{3,4}

¹ Yunnan Observatories, Chinese Academy of Sciences, Kunming 650011, People's Republic of China; nanbin@ynao.ac.cn

² Key Laboratory of Dark Matter and Space Astronomy, Purple Mountain Observatory, Nanjing 210008, People's Republic of China

³ School of Earth and Space Sciences, Peking University, Beijing 100871, People's Republic of China

⁴ State Key Laboratory of Space Weather, Chinese Academy of Sciences, Beijing 100190, People's Republic of China

⁵ Key Laboratory of Solar Activity, National Astronomical Observatories, CAS, Beijing 100012, People's Republic of China

Received 2019 November 25; revised 2020 May 7; accepted 2020 May 7; published 2020 June 9

Abstract

The daily interplanetary magnetic field (IMF) B_x , B_y , and B_z components from 1967 January 1 to 2018 December 31 listed in the OMNI database are used to investigate their periodicity and study temporal variation of their rotation cycle lengths through continuous wavelet transform, autocorrelation, and cross-correlation analyses. The dominant rotation period in each of the daily B_x , B_y , and B_z components is 27.4 days, implying the existence of rotational modulation in the three time series. The dependence of the rotation cycle lengths for both B_x and B_y components on solar cycle phase almost shows the same result. The rotation cycle lengths for both B_x and B_y components increase from the start to the first year of a new Schwabe cycle, then decrease gradually from the first to the fourth year, and finally fluctuate around the 27.4-day period within a small amplitude from the fourth year to the end of the Schwabe solar cycle. For the B_z component, its rotation cycle length does not show such a solar cycle variation. The significant periods in the variation of B_x rotation are 2.9, 3.4, 4.3, 4.9, 10.5, and 11.9 yr, and there exist significant periods of 3.4, 9.9, and 14.1 yr in the variation of B_y rotation. The relationship of solar activity with B_x and B_y components is complex. The possible mechanisms for the temporal variation of the rotation period of the three components are discussed.

Unified Astronomy Thesaurus concepts: [Interplanetary magnetic fields \(824\)](#)

1. Introduction

The interplanetary magnetic field (IMF) is the solar magnetic field carried out by solar wind. Observations recorded by various spacecraft near Earth show that the IMF intensity is generally lower than 10 nT. Thus, compared with the magnetic field strength on the solar surface, the intensity of the IMF near Earth is very low. However, the IMF is one of the critical factors of space weather, and major space disturbances such as magnetic storms and substorms are due to IMF effects. When the IMF encounters the geomagnetic field, with an opposite direction, magnetic reconnection can help, and thus the enhanced interaction can cause intense substorms/convection events and even produce severe space weather conditions, which may affect the manned and unmanned space missions, navigation, power lines, telecommunications, etc. (Dungey 1961; Gonzalez & Mozer 1974; Gonzalez et al. 1994; Gopalswamy et al. 2007; Pulkkinen 2007; Badruddin & Kumar 2015).

The temporal variation and dynamical evolution of the IMF and its components near Earth had been studied extensively ever since it was observed by different spacecraft (Gonzalez & Gonzalez 1987; Cane et al. 1998; Neugebauer et al. 2000; Prabhakaran Nayar et al. 2002; Takalo & Mursula 2002; Mursula & Vilppola 2004; Singh et al. 2012; Chowdhury et al. 2015; Souza et al. 2016). Especially, an enormous amount of research focused on investigations of the rotation period of the IMF or its B_x , B_y , and B_z components (e.g., Neugebauer et al. 2000; Takalo & Mursula 2002; Katsavrias et al. 2012; Vats 2012; Singh et al. 2012; Chowdhury et al. 2015; Xiang & Qu 2018; Choi & Lee 2019; Singh & Badruddin 2019; Tschla et al. 2019), because the (differential) rotation in the solar interior is linked to the solar dynamo, and the rotation signal, as one of the most prominent oscillations in various

solar activity indicators, can be found from the solar interior to the interplanetary space. The IMF originates from the Sun, and the solar magnetic field on the solar surface should be thought to be critical in determining the nature of the rotation period of the IMF and its components. Therefore, clearly understanding the relation between IMF/its components and solar magnetic field can help us to further comprehend the nature of the IMF and its components and assess the influence of the solar magnetic field on them.

The data of the daily IMF polarity during the time interval of 1926–1982 were utilized by Gonzalez & Gonzalez (1987) to analyze its periodicity, and they found a significant rotation period of about 27.5 days, which changes from about 28 days at the beginning of a solar cycle to about 27 days at the end of the cycle. A rotation period of about 27.03 days was detected in the radial IMF component by Neugebauer et al. (2000), and the authors specifically suggested that such a period is the most dominant rotation period during the time interval of 1962–1998 and should be due to the preferred-longitude effects. A similar study that was given by Takalo & Mursula (2002) proposed the existence of the most persistent synodic solar rotation of about 27.6 days in the IMF B_x component in geocentric solar ecliptic (GSE) coordinates during 1964–1995. Several authors also reported that the significant rotation cycle of about 27.0 days was detected in the IMF B_y component (Katsavrias et al. 2012; Choi & Lee 2019; Tschla et al. 2019). At the same time, the method of the auto-covariance function proposed by Takalo & Mursula (2002) showed that the auto-covariance function of the IMF B_y component is very similar to that of the IMF B_x component, indicating that B_x and B_y have the same rotation period. A similar result can also be found in Katsavrias et al. (2012) and Choi & Lee (2019), but the rotation period of B_x

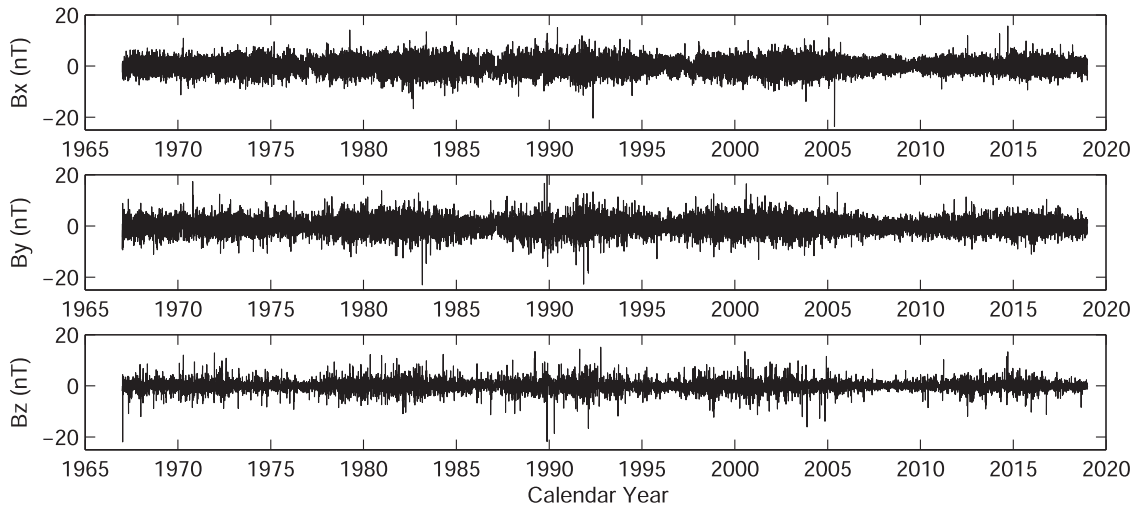


Figure 1. Daily IMF B_x component (top panel), daily IMF B_y component (middle panel), and daily IMF B_z component (bottom panel) from 1967 January 1 to 2018 December 31.

and B_y given by different authors has a small difference, which may be caused by the different analysis methods used. For instance, the rotation period of B_x and B_y obtained by wavelet analysis is 27.8 days, while it is 27 days as detected by the Lomb–Scargle algorithm (Katsavrias et al. 2012). The rotation period of the IMF B_z component is different from that of the IMF B_x and B_y components. Katsavrias et al. (2012) advised that the rotation period of B_z is 28 and 30 days, and Chowdhury et al. (2015) found that the Lomb–Scargle periodogram of the B_z component in GSE coordinates displays significant rotation periods of about 20, 26, 29, 30, 32, and 34 days, but the rotation period of the B_z component in geocentric solar magnetospheric (GSM) coordinates is found to be 28.5 days by Tschla et al. (2019). The IMF B_z component in GSM exhibits the maximum southward possibility around spring equinox when IMF is toward the Sun, and such a maximum is found around fall equinox when IMF is away from the Sun. This is the well-known Russell–McPherron effect (Russell & McPherron 1973), which can influence the periodic behavior of B_z in GSM. Choi & Lee (2019) further studied the origin and temporal evolution of the rotation period and harmonics in the IMF B_z component and found that a seasonal dependence of the rotation period in the B_z component in GSM is seen primarily during the northern hemisphere spring and fall seasons. This result is due to an exquisite harmony between the Russell–McPherron effect and the IMF sector structure that displays either two or four sectors for a long time interval. In terms of the rotation period in IMF intensity, many studies found the existence of a synodic solar rotation period of about 27 days in IMF intensity and also found that the rotation period varies from one solar cycle to the next (Prabhakaran Nayar et al. 2002; Singh et al. 2012; Vats 2012; Singh & Badruddin 2019).

In a word, the rotation period of the IMF and its components is slightly different from different studies, since different mathematical methods and time series during different time intervals were adopted in these studies. However, it is widely agreed that the rotation period in IMF intensity and its B_x , B_y , and B_z components vary with solar activity, but there are few studies on the temporal variation of their rotation periods. One can see that previous studies mainly focused on detecting the rotation period of the IMF intensity and its components during a certain time interval, and thus the rotation period obtained in

these studies represented a mean result while omitting the temporal variation of the rotation period. On the other hand, Choi & Lee (2019) studied the origin and temporal evolution of the rotation period in the IMF B_z component during solar cycles 23–24, but the authors mainly focused on the cause of the seasonal variation in this component. Xiang & Qu (2018) showed that the rotation period of the IMF intensity appears intermittently around the solar maximum times, and Singh & Badruddin (2019) further investigated the temporal evolution of the rotation period in IMF intensity during epochs of the polarity reversal of solar cycles 20–24. Furthermore, the temporal variation of solar rotation determined from different solar activity indicators that are located at different heights in the solar atmosphere from the photosphere to corona has been studied extensively in early studies (Javaraiah & Gokhale 1995; Brajša et al. 2006; Li et al. 2012; Xie et al. 2017b). Following these studies, we will further investigate the temporal evolution of the rotation periods in IMF B_x , B_y , and B_z components, which will show a clear variation of rotation period with solar activity on different timescales and further enable us to better understand the relation between IMF and the solar magnetic field.

2. Data and Methods

The IMF and its components have been recorded at the OMNI (Operating Missions as a Node on the Internet) database of NASA since 1963, which are based on the systematical observation by various spacecraft in near-Earth orbits. However, there are too many data gaps during 1963–1966, in which data gaps are sometimes longer than 27 days, which are adverse to analyzing the rotation period. Thus, only the daily IMF B_x , B_y , and B_z components in GSM from 1967 January 1 to 2018 December 31 are used in this study, which can be downloaded from the website of the OMNI database of NASA (<https://omniweb.gsfc.nasa.gov/form/dx1.html>). The daily IMF B_x , B_y , and B_z components are shown in Figure 1, from which the pronounced solar activity cycle can be hardly seen.

The wavelet analysis can reveal the periodic variations and the localized oscillatory feature of a time series in two-dimensional time–frequency space, and thus it is widely used to detect dominant periods of a time series at different timescales and exhibit a localized oscillatory feature in time–frequency

space (Torrence & Compo 1998; Grinsted et al. 2004; Chowdhury & Dwivedi 2011; Deng et al. 2013; Xie et al. 2017a). Accordingly, this method is suitable for studying the temporal evolution of the rotation period in IMF B_x , B_y , and B_z components. We use the wavelet for feature extraction purposes, and a reasonable localization in both time and frequency is needed. Thus, it is a logical and pragmatic choice to use the Morlet wavelet (dimensionless frequency $\omega_0 = 6$) in this study (Torrence & Compo 1998; Deng et al. 2016). The continuous wavelet transform (CWT) is used to analyze the periods of IMF B_x , B_y , and B_z components. This method is described in detail in Grinsted et al. (2004) and Li et al. (2009). However, the observation data are finite-length time series; the result of CWT may be artifacts at the beginning and end of the wavelet power spectrum. One solution to this problem is to introduce a cone of influence (COI) in which edge effects become important. For a discontinuity at the edge, the wavelet power decreases by a factor e^{-2} (Torrence & Compo 1998; Grinsted et al. 2004; Xie et al. 2012).

The autocorrelation analysis is widely used to investigate the temporal variation of the rotation cycle lengths of the solar activity indicators in early studies (Chandra & Vats 2011; Xiang et al. 2014; Xie et al. 2017a), and thus we also use this method to analyze the temporal variation of the rotation cycle lengths for IMF B_x , B_y , and B_z components. The autocorrelation analysis is simply described as follows. The daily observation of a solar activity indicator can be represented in the form of a time series $\{x_1, x_2, \dots, x_n\}$, where index 1, 2, ..., n represents the first, second, ..., last element, respectively. If this time series x shifted by d days with respect to itself, we can obtain $(n - d)$ pairs of values from this series, $(x_1, x_{d+1}), (x_2, x_{d+2}), \dots, (x_{n-d}, x_n)$. Then, the first value and the second value in each pair can be considered as the first variable $\{x_1, x_2, \dots, x_{n-d}\}$, the second variable $\{x_{d+1}, x_{d+2}, \dots, x_n\}$, respectively. The autocorrelation coefficient $P(d)$ as a function can be defined as (Chandra & Vats 2011)

$$P(d) = \frac{\sum_{i=1}^{n-d} (x_i - \bar{x})(x_{i+d} - \bar{x})}{\sum_{i=1}^{n+1-d} (x_i - \bar{x})^2}, \quad (1)$$

where \bar{x} is the mean of this time series (daily observations) and x_i indicates the i th element of time series $\{x_1, \dots, x_n\}$.

The cross-correlation analysis, which is widely used to investigate the mutual correlation and phase relationship between two time series (Edelson & Krolik 1988; Chandra & Vats 2011; Xu & Gao 2016), is utilized to further analyze the relation of the rotation cycle lengths of the IMF components with solar activity in this study. We assume the daily observations of two solar activity indicators with an equal length, $\{x_1, x_2, \dots, x_n\}$ and $\{y_1, y_2, \dots, y_n\}$. The cross-correlation coefficient $ccc(k)$ between two time series is defined as (Chandra & Vats 2011; Xu & Gao 2016)

$$ccc(k) = \begin{cases} \frac{\sum_{i=1}^{n+k} (x_{i-k} - \bar{x})(y_i - \bar{y})}{\sqrt{\sum_{i=1}^{n+k} (x_{i-k} - \bar{x})^2 \sum_{i=1}^{n+k} (y_i - \bar{y})^2}}, & k < 0 \\ \frac{\sum_{i=1}^{n-k} (x_i - \bar{x})(y_{i+k} - \bar{y})}{\sqrt{\sum_{i=1}^{n-k} (x_i - \bar{x})^2 \sum_{i=1}^{n-k} (y_{i+k} - \bar{y})^2}}, & k \geq 0 \end{cases}, \quad (2)$$

where x_i and y_i indicate the i th element of data sets $\{x_1, \dots, x_n\}$ and $\{y_1, \dots, y_n\}$, respectively, and \bar{x} and \bar{y} are the mean of the daily observations of the two solar activity indicators. The k

indicates the shift of x versus y along the calendar-time axis, with negative values representing backward shifts.

3. Temporal Evolution of the Rotation Period in IMF B_x , B_y , and B_z Components

3.1. Periods of IMF B_x , B_y , and B_z Components

The data gaps in IMF B_x , B_y , and B_z components during the time interval we considered are interpolated through the linear interpolation method. Especially in the 1980s, the relatively long and systematic gaps that may be referred to the effect of the magnetospheric parts of the spacecraft orbit can be found in the OMNI database. However, the continuous data gaps in three time series are generally shorter than 6 days, which is much shorter than the rotation period of about 27 days. Thus, the data gaps have little effect on the analysis of the rotation period after data gap interpolation. Then, we use the CWT to analyze the periodicities of IMF B_x , B_y , and B_z components, and the results are shown in Figure 2. In this figure, the left column shows the continuous wavelet power spectra of the daily B_x , B_y , and B_z components from 1967 January 1 to 2018 December 31, where their corresponding 95% confidence level is indicated by the thick black contours. At the same time, we calculate the time-averaged wavelet spectrum based on the local ‘‘components’’ of continuous wavelet power spectra over all time intervals considered, which is the global power spectra and can help to identify the dominant periods. The global power spectra of the three time series and their corresponding 95% confidence level are shown in the right column of this figure.

The left column of this figure shows that the rotation period of about 27 days in both IMF B_x and B_y components is of statistical significance almost throughout the entire time interval considered, but the periodic variation in IMF B_z on timescales of a solar rotation cycle is intermittent; such a case is more obvious during solar cycles 23 and 24. The period of about 13 days in the three time series, which may be the 1/2 multiple harmonic of the rotation period, is intermittently detected around the sunspot maximum times. The global power spectra indicate that the possible periods for the IMF B_x component are 13.7, 27.4, and 184.3 days and 1.01, 3.45, 7.40, and 11.25 yr, but only the periods of 13.7 and 27.4 days and 1.01 yr are above the 95% confidence level. For the IMF B_y component, the periods of 13.7 and 27.4 days and 1.02 and 7.0 yr are of statistical significance; some possible periods for this time series are 187.0 days and 2.37 and 10.94 yr, but the peak powers corresponding to these periods are below the 95% confidence level. The statistical significant periods for the IMF B_z component that are above the 95% confidence level are 13.9 and 27.4 days and 0.9 and 7.74 yr, and the possible periods for this time series but whose peak powers are below the 95% confidence level are 101.9 and 184.3 days and 1.58 and 2.77 yr.

The rotation period for all three time series of IMF B_x , B_y , and B_z components is about 27.4 days, and the periods of 13.7 days in B_x and B_y and 13.9 days in B_z should be the first solar rotation harmonics. The results obtained from wavelet analysis are consistent with early studies (Takalo & Mursula 2002; Katsavrias et al. 2012; Choi & Lee 2019; Tschla et al. 2019). The periods indicated by the global power spectrum peaks should represent a mean result over a specific time interval, and they indicate the most dominant periods at specific timescales in the entire time interval considered.

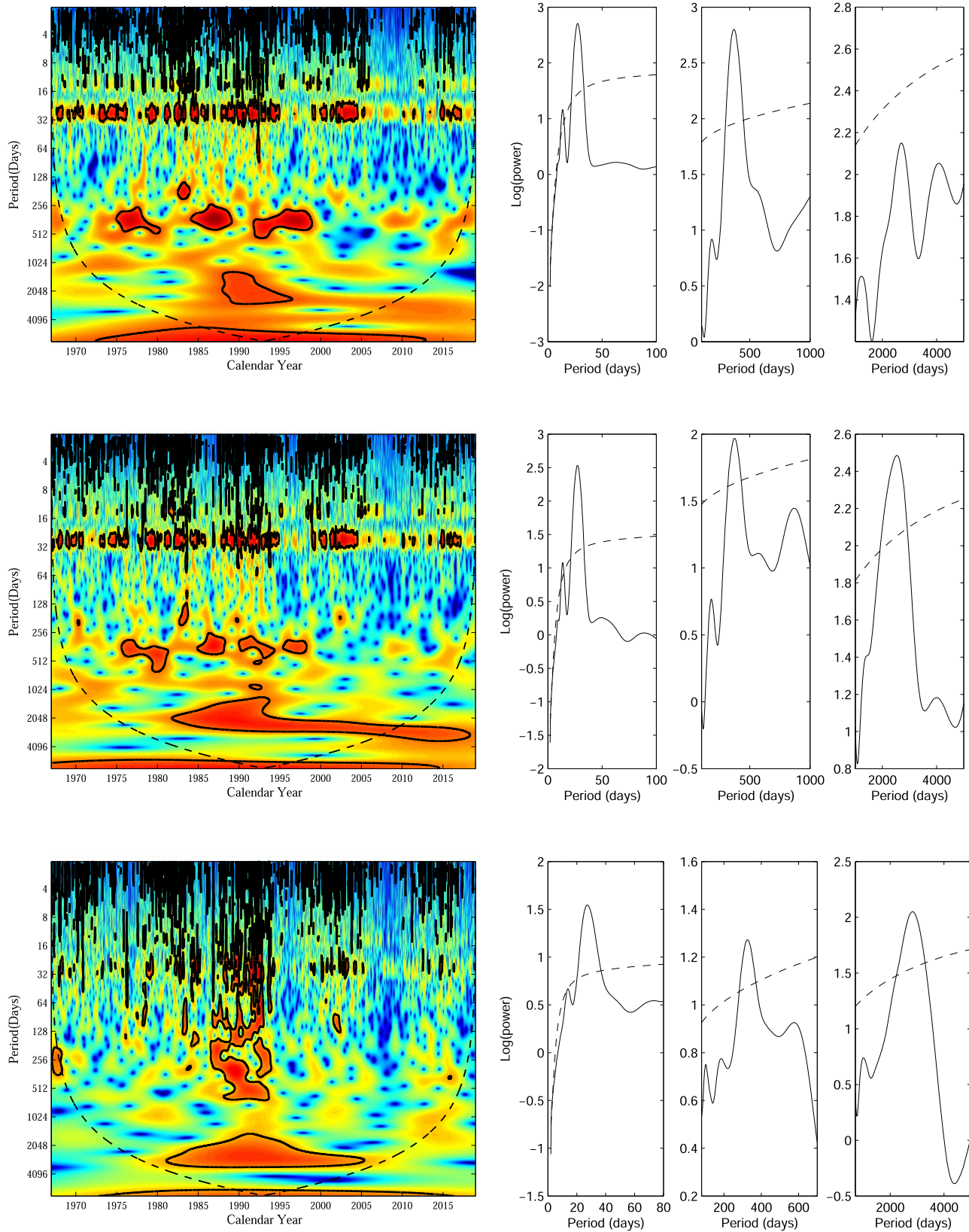


Figure 2. Left column: continuous wavelet power spectra of the daily B_x (top panel), B_y (middle panel), and B_z (bottom panel) components from 1967 January 1 to 2018 December 31. The thick black contours and the black dashed line in each panel indicate the 95% confidence level and the COI, respectively. Right column: global wavelet power spectra (solid line) and the 95% confidence level (dashed line) of the daily B_x (top panel), B_y (middle panel), and B_z (bottom panel) components.

Consequently, the most dominant rotation period for all three time series of B_x , B_y , and B_z in 1967–2018 is 27.4 days. On the timescales of several months to years, the significant periods

are 1.01 yr in B_x , 1.02 yr in B_y , and 0.9 yr in B_z . Early studies proved that the periods on timescales of 0.6 to 4 yr found in various solar activity indicators are often considered as

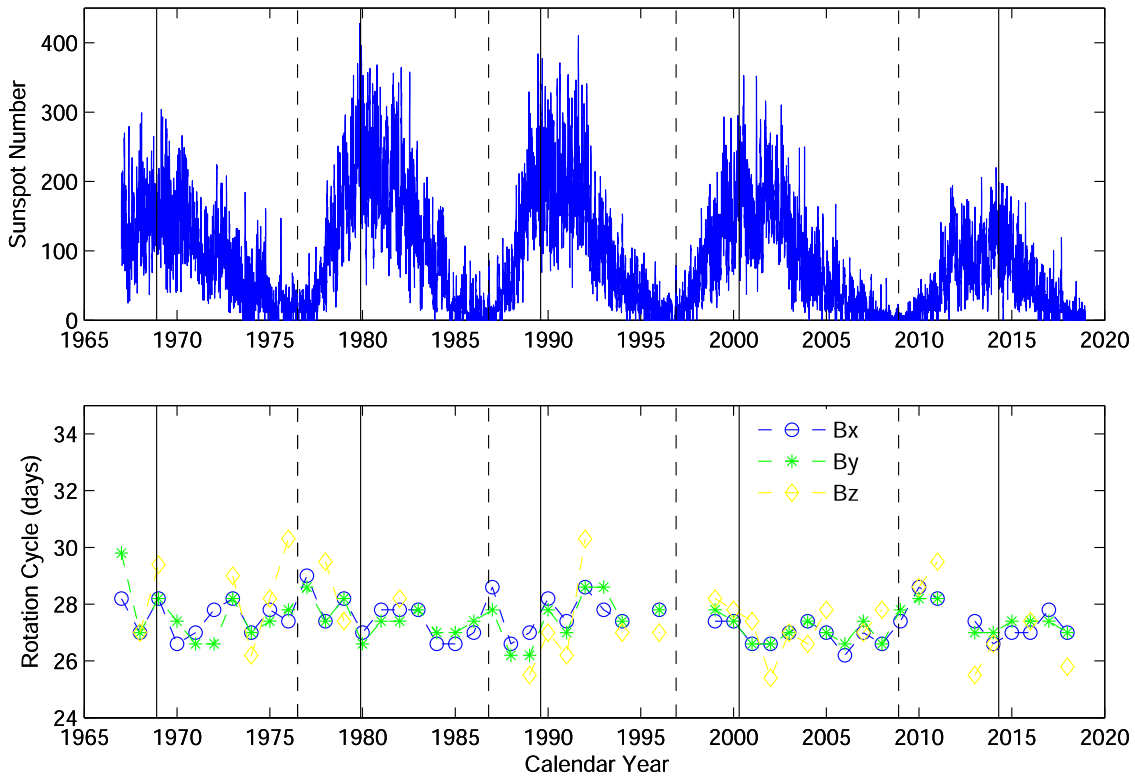


Figure 3. Top panel: daily sunspot number from 1967 January 1 to 2018 December 31. Bottom panel: rotation cycle lengths of the daily IMF B_x component (blue dashed line with circles), the daily IMF B_y component (green dashed line with asterisks), and the daily IMF B_z (yellow dashed line with diamonds) in each year of the entire time interval we considered. The maximum and minimum times of sunspot cycles are indicated by the vertical solid and dashed lines in each panel, respectively.

quasi-biennial oscillations (QBOs), which should be derived from the base of the solar convection zone and are visible from the base of the solar convection zone in the solar interior to the interplanetary space (Bazilevskaya et al. 2000, 2014; Bumba 2003; Kane 2005; Vecchio et al. 2012; Xiang 2019). Hence, these periods on timescales of about 1 yr found in IMF B_x , B_y , and B_z components are also considered as QBOs, which should be related to the solar QBOs. The significant periods are 7.0 yr for B_y and 7.74 yr for B_z , two of which should be the 1/3 multiple harmonics of the quasi-22 yr magnetic activity cycle. Additionally, the Schwabe solar cycle of about 11 yr for three time series is statistically insignificant; this result is consistent with Figure 1, from which the pronounced solar activity cycle can be hardly seen.

3.2. Dependence of the Rotation Cycle Lengths of the IMF B_x , B_y , and B_z Components on the Solar Cycle Phase

In order to further study the temporal variation of the rotation cycle lengths of the IMF B_x , B_y , and B_z components in the entire time interval considered, we detect the rotation cycle lengths of the three time series in each year, respectively. First, we cut the daily B_x component (B_y and B_z components) during the entire time interval we considered into yearly time series, each of which is from the first day of that calendar year to the last day of that calendar year. Then, the CWT is again utilized to determine the rotation period for each of the yearly time series, and only those periods that are above the 95% confidence level are taken into account. The rotation cycle lengths of the daily B_x , B_y , and B_z components in each year are obtained, and the results are shown in Figure 3. In order to better visualize possible solar cycle effects, the daily sunspot number during the same time interval is also given in Figure 3.

As this figure shows, both daily B_x and B_y span 52 yr from 1967 to 2018, and 48 values of the rotation period that are above the 95% confidence level are detected for each yearly time series of the IMF B_x and B_y components. In 1995, 1997, 1998, and 2012, which are in the minimum time or ascending phase of sunspot cycles, the rotation period for both daily B_x and B_y is statistically insignificant. However, only 30 values of rotation period are found above the 95% confidence level for yearly time series of the IMF B_z components in the total 52 yr. The rotation cycle lengths of the IMF B_x and B_y components show almost the same temporal variation during the time interval considered, and in each solar cycle they seem longer near the solar minimum than near the solar maximum. But the rotation cycle lengths of the IMF B_z component display different temporal variation, and the rotation period is missing in too many years to visualize the possible solar cycle effect. Moreover, the rotation cycle lengths for daily B_x , B_y , and B_z components are determined to be 27.4 ± 0.66 days, 27.4 ± 0.71 days, and 27.6 ± 1.37 days, respectively. The rotation cycle length for both B_x and B_y components is found to fluctuate around the most dominant rotation period of 27.4 days with a very small amplitude, but the temporal variation of the rotation cycle length of the B_z component shows a rather larger amplitude.

Based on the rotation cycle length of the IMF B_x (B_y) component in each year of the entire time interval we considered, we can further study the dependence of the rotation cycle lengths of the two time series on the solar cycle phase. We calculate the average of the rotation cycle length of the IMF B_x (B_y) component in each year within the same sunspot cycle phase relative to the nearest preceding sunspot cycle minimum, and the obtained result is shown in Figure 4. In the figure, error

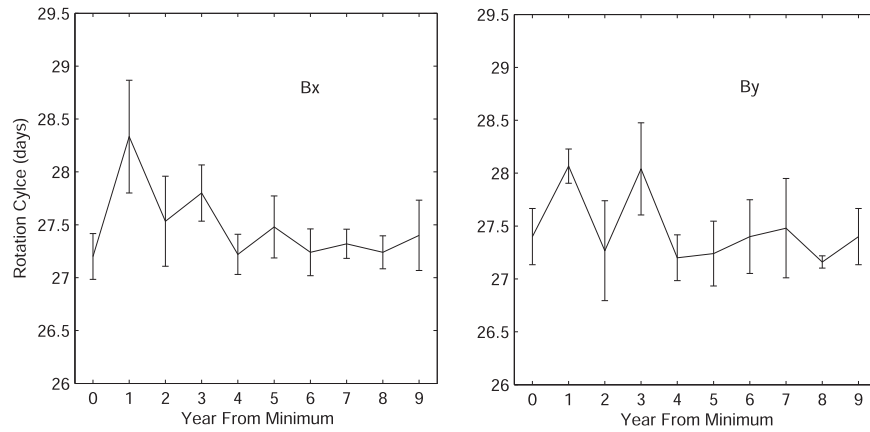


Figure 4. Dependence of rotation cycle length for the daily B_x component (left panel) and the daily B_y component (right panel) on the solar cycle phase. Error bars in each panel indicate the corresponding standard errors.

bars are utilized to indicate the corresponding standard errors (σ). As this figure displays, the profile of the rotation cycle length of the B_x component is almost the same as that of the B_y component. The rotation cycle lengths for both B_x and B_y increase from the start to the first year of a new Schwabe cycle, then decrease gradually from the first to the fourth year of the Schwabe cycle, and finally fluctuate around the 27.4-day period within a small amplitude from the fourth year to the end of the Schwabe solar cycle. According to the difference of the rotation cycle lengths of the IMF B_x (B_y) component and the corresponding standard errors σ , a simple method of the 3σ rule is used to assess the statistical significance of variations of the rotation cycle lengths for B_x and B_y components. Generally, one can see that the variations of the rotation cycle lengths between two adjacent years for the B_x (B_y) component are consistent with the corresponding σ , even smaller than the corresponding σ . This indicates that the variations of two adjacent rotation cycle lengths should be statistically insignificant. However, it can be found that the variations between the maximum and minimum values of the rotation cycle lengths for the IMF B_x (B_y) component are larger than the corresponding 2σ , which indicates that such variations are above the 95% confidence level. Hence, the decrease of the rotation cycle lengths for B_x (B_y) is statistically significant, and the profile of rotation cycle lengths shown in Figure 4 can to some extent truly reflect the dependence of the rotation cycle lengths for the B_x (B_y) component on the solar cycle phase.

For the IMF B_z component, the rotation period is missing in too many years during the time interval considered, and thus we cannot use this method to study the dependence of the rotation cycle length for B_z on the solar cycle phase. However, the local wavelet power spectra of the B_z component (Figure 2) have the highest spectral power peaks at a certain day on the rotation timescales of 22–32 days, and thus we can select these highest spectral power peaks that are above the 95% confidence level, which can be used to determine the significant rotation period of the B_z component at each day during the entire interval we considered. The result is shown in the bottom panel of Figure 5. Meanwhile, the daily sunspot number during the same time interval is given in the top panel of the figure, which can help to better visualize possible solar cycle effects. As this figure shows, the significant rotation cycle lengths for B_z display random and complex variations, and they appear intermittently during the entire time interval we considered. Both the longest and shortest rotation cycle lengths for the B_z

component seem to appear in an arbitrary phase of solar cycles, and thus we cannot determine whether the rotation cycle lengths around the solar maximum time should be longer or shorter than those around the minimum time. This may indicate that the dependence of the rotation cycle length for the B_z component on the solar cycle phase does not have the cycle-related variation.

3.3. Periodicity in the Temporal Variation of the Rotation Cycle Lengths of the IMF B_x and B_y Components

The continuous wavelet power spectra of the daily IMF B_x , B_y , and B_z components shown in Figure 2 can indicate the localized oscillatory feature. As this figure shows, the local wavelet power spectra of the B_x (B_y) component have the highest spectral power peaks at a certain day on the rotation timescales of 22–30 days, and thus these highest spectral power peaks can be used to determine the rotation period of the B_x (B_y) component at each day during the entire time interval considered. Early study in Katsavrias et al. (2012) also pointed out that the rotation period of 22–30 days (peaks at 27.8 days) appears in both IMF B_x and B_y during 1966–2010. But for the IMF B_z component, Figure 3 shows that the rotation period for the B_z component is missing in 22 yr of the total 52 yr, and Figure 5 also shows that the significant rotation period for B_z appears intermittently during the entire time interval we considered; such case is more obvious during solar cycles 23 and 24. Thus, we cannot further investigate the periodicity in the temporal variation of the B_z rotation. The obtained rotation periods of the B_x (B_y) component during the time interval considered are smoothed by the sliding average of 1 yr, and then we can obtain two new time series as shown in Figure 6, which are named RCL_x and RCL_y and should show the variations of the rotation cycle lengths in B_x and B_y components with solar activity, respectively. As this figure shows, the rotation cycle lengths for both B_x and B_y vary on the timescales of more than 1 yr to a Schwabe solar cycle. In each solar cycle, the longest rotation cycle length for both B_x and B_y seems to occur near 1 yr after the start of a Schwabe solar cycle except for solar cycle 22, while the shortest rotation cycle of two time series seems to always appear near the solar maximum times. Additionally, these extrema near the start and end of the time interval considered may have suffered from edge artifacts, which should not indicate the true rotation cycle lengths.

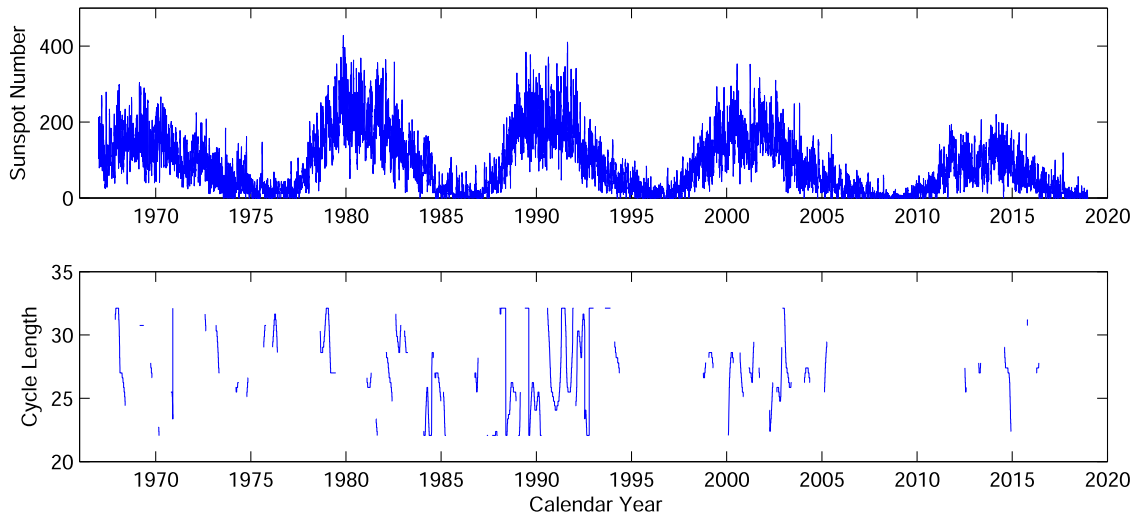


Figure 5. Top panel: daily sunspot number from 1967 January 1 to 2018 December 31. Bottom panel: temporal variation of the significant rotation period of the B_z component in the same time interval.

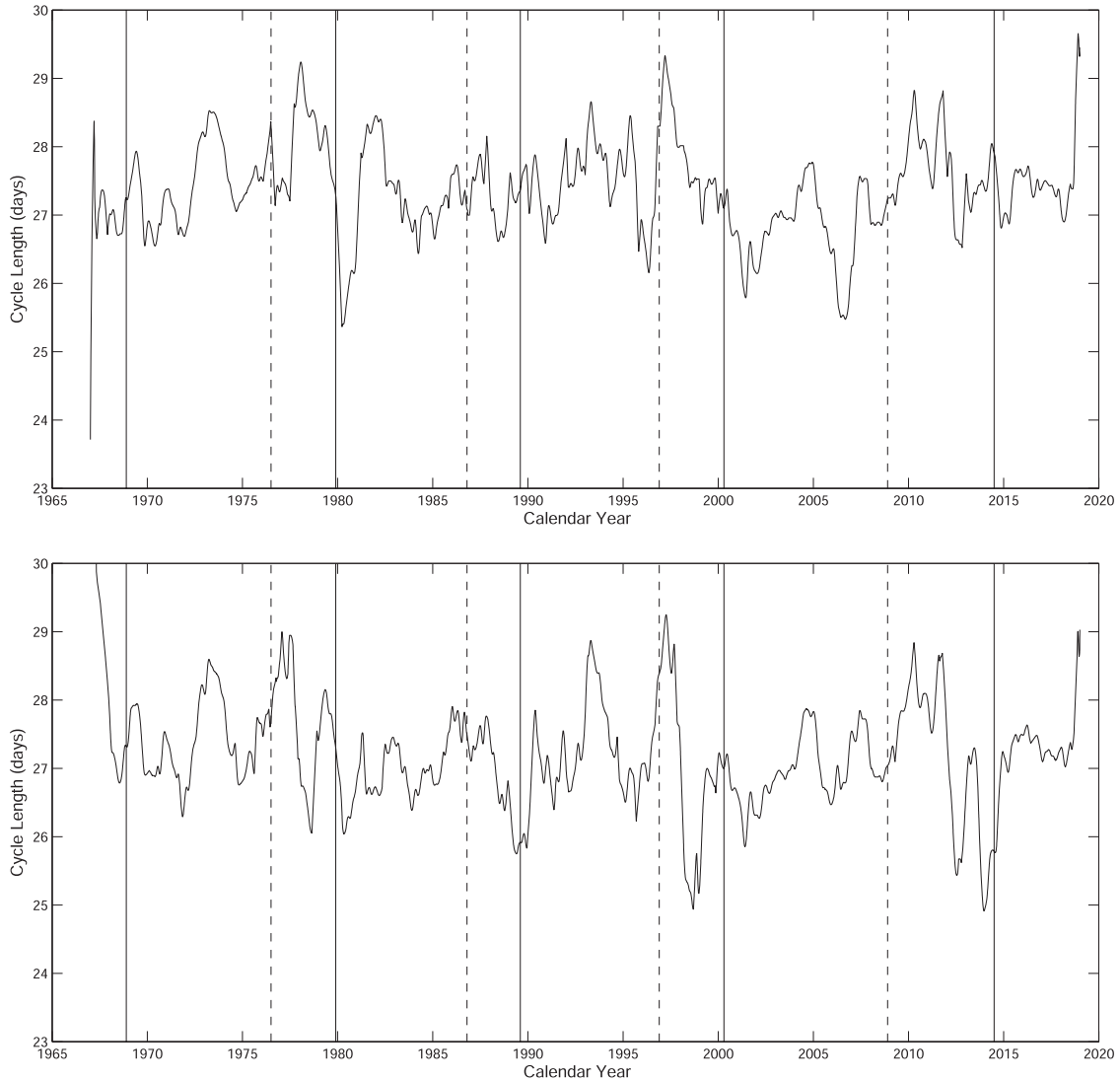


Figure 6. Temporal variation of B_x rotation (top panel) and B_y rotation (bottom panel) from 1967 January 1 to 2018 December 31. The maximum and minimum times of sunspot cycles are indicated by the vertical solid and dashed lines, respectively.

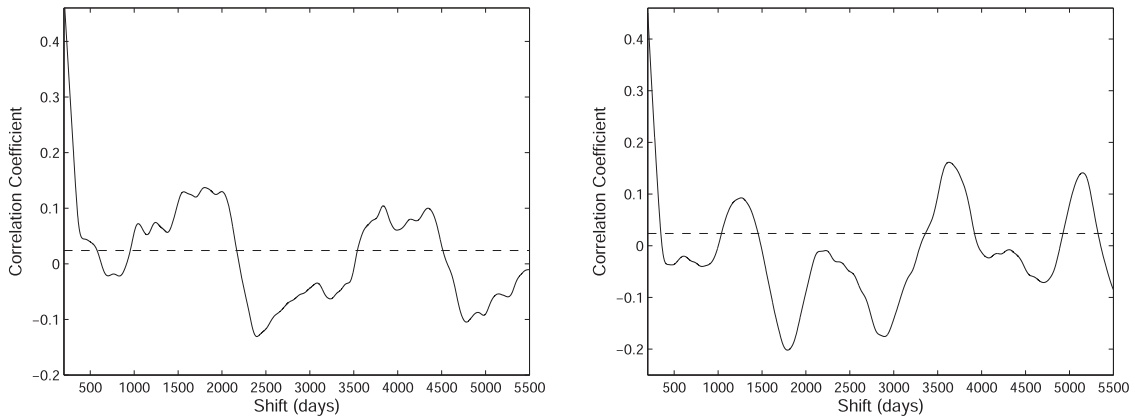


Figure 7. Left panel: autocorrelation coefficients of relative phase shifts of RCL_x with respect to itself for 200–5500 days. Right panel: same as the left panel, but for autocorrelation analysis of RCL_y . The 99.9% confidence level is indicated by the dashed horizontal line in each panel.

We use the autocorrelation analysis to further study the periods of the temporal variation of the rotation cycle lengths of the IMF B_x and B_y components. The autocorrelation coefficients ($P(d)$) of RCL_x/RCL_y with respect to itself are calculated, varying with relative shifts in 1–5500 days. In order to clearly show peaks, Figure 7 just shows the $P(d)$ for 200–5500 days. At the same time, the 99.9% confidence level is also indicated by the dashed horizontal line. As this figure shows, the periods for the rotation cycle lengths of the B_x component are 2.9, 3.4, 4.3, 4.9, 10.5, and 11.9 yr, and they are statistically significant at the 99.9% confidence level. The periods at the 99.9% confidence level for the rotation cycle lengths of the B_y component are 3.4, 9.9, and 14.1 yr. Those midterm periods of 2.9, 3.4, 4.3, and 4.9 yr may be related to the multiscale magnetic activity in the solar atmosphere. The periods of about 9.9, 10.5, and 11.9 yr detected in RCL_x or RCL_y indicate that the variation of the rotation cycle lengths of the IMF B_x and B_y components may be related to the 11 yr solar activity cycle. Additionally, the period of 14.1 yr found in RCL_y is longer than the solar cycle length, which hints that the variation of the rotation cycle lengths of this time series may have some relation to the extended activity cycle.

3.4. Relation of the Rotation Cycle Lengths of the IMF B_x and B_y with Solar Activity

The sunspot number is the most common indicator that describes the solar activity level, and it was widely used in early studies (Chernosky & Hagan 1958; Cole 1973; Hathaway et al. 1994; Hathaway 2015; Gao 2016). The daily sunspot numbers from 1967 to 2018, which are downloaded from the website of the Solar Influences Data Analysis Center (<http://sidc.oma.be/silso/>), are used to study the relation of the rotation cycle lengths of the IMF B_x and B_y components with solar activity.

The sunspot numbers from 1967 January 1 to 2018 December 31 are also smoothed by the sliding average of 1 yr, and the time series of the 1 yr smoothed daily sunspot numbers is obtained, which is named SSN. Then, we perform a cross-correlation analysis of RCL_x/RCL_y versus SSN, and the results are shown in Figure 8. In this figure, the abscissa represents shifts of RCL_x/RCL_y with respect to SSN along the calendar-time axis, and the negative values indicate that RCL_x/RCL_y lags behind SSN. As the left panel of this figure shows, the cross-correlation coefficient (ccc) is 0.08 at no shift,

while it reaches a maximum of 0.18 when RCL_x is shifted forward by about 2.7 yr. The maximum is located outside the dashed horizontal lines; it is thus statistically significant at the 99% confidence level. At the same time, the ccc shows a local minimum of -0.30 when RCL_x is shifted backward by about 1.2 yr, and the local minimum is also statistically significant at the 99% confidence level. We do not analyze the difference between the maximum positive correlation (0.18) and the local minimum negative correlation (-0.30). However, both the forward shift and backward shift indicate that there is a phase difference between the rotation cycle lengths of the B_x component (RCL_x) and solar activity (SSN). Another local peak appears to be -0.04 when RCL_x is shifted backward by about 7.9 yr, which is also statistically significant at the 99% confidence level. The phase shift between two adjacent peaks is about 10.6 yr, which is consistent with the period in the rotation cycle lengths of the B_x component (10.5 yr). Thus, the cross-correlation analysis demonstrates that the rotation cycle lengths of the B_x component have a period of about 10.5 yr. The cross-correlation analysis of RCL_y versus SSN shows similar results. As the right panel of Figure 8 displays, the ccc peaks at 0.26 when RCL_y is shifted forward by about 5.0 yr and shows a local minimum of -0.34 at the shift of about -0.5 yr. Thus, both the peak and local minimum suggest the existence of a phase difference between the rotation cycle lengths of the B_y component (RCL_y) and solar activity (SSN). Additionally, a local maximum of ccc can be found at the shift of about -4.9 yr. The phase shift between the two peaks is about 9.9 yr, which is the same as the period in the rotation cycle lengths of the B_y component. Consequently, this result validates that there exists a 9.9 yr period in rotation cycle lengths of the B_y component.

4. Discussions and Conclusion

The daily IMF B_x , B_y , and B_z components from 1967 January 1 to 2018 December 31 listed in the OMNI database are used to investigate their periodicity using the continuous wavelet transform, and then we further study the temporal variation of the rotation cycle lengths of the three time series during the time interval we considered.

The continuous wavelet power analysis of the daily IMF B_x , B_y , and B_z components suggests that the significant periods are 13.7 and 27.4 days and 1.01 yr for B_x , 13.7 and 27.4 days and 1.02 and 7.0 yr for B_y , and 13.9 and 27.4 days and 0.9 and 7.74

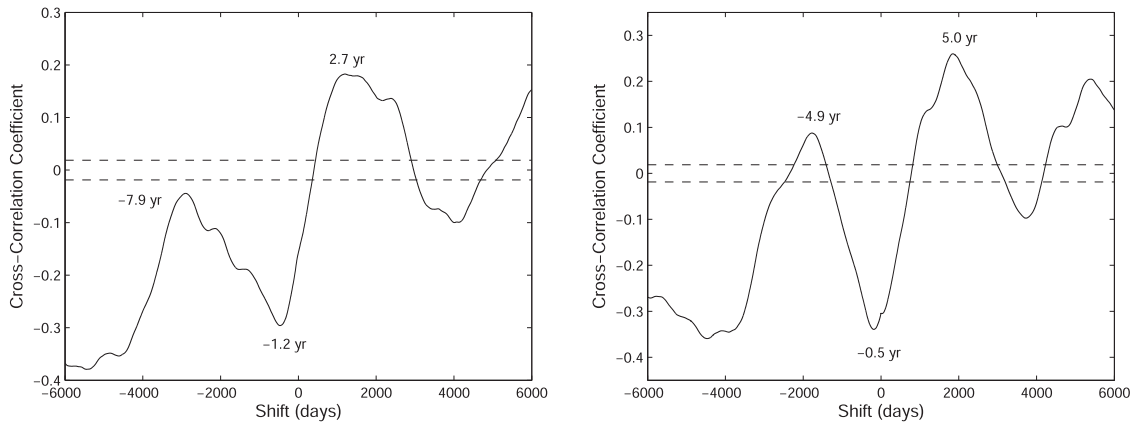


Figure 8. Left panel: cross-correlation coefficients of RCL_x vs. SSN. The abscissa represents shifts of RCL_x with respect to SSN along the calendar-time axis, and the negative values indicate that the RCL_x lags behind SSN. The two dashed horizontal lines indicate the corresponding value at the 99% confidence level. Right panel: same as the left panel, but for RCL_y vs. SSN.

yr for B_z , and thus the temporal variation of daily IMF B_x , B_y , and B_z components is modulated by multiscale variability of solar activity. Additionally, the Schwabe solar cycle of the three time series is statistically insignificant, which implies that the temporal variation for the daily IMF B_x , B_y , and B_z components should not be related to the 11 yr solar cycle.

The continuous wavelet power spectra displayed in Figure 2 show that the oscillation periods in both the B_x and B_y components on the timescales of a solar rotation period are of statistical significance almost throughout the entire time interval we considered. But for the B_z component, such oscillation periods are found to intermittently appear. The global power spectra shown in this figure indicate that the rotation period in the three time series is 27.4 days. The value of the rotation period is very consistent with the result in Takalo & Mursula (2002), in which the authors proposed the existence of the most persistent synodic solar rotation of about 27.6 days in the IMF B_x component during 1964–1995. Katsavrias et al. (2012) also investigated the rotation periods by applying the continuous wavelet transform to the daily IMF B_x , B_y , and B_z components during 1966–2010 and found a rotation period of 27.8 days in the three time series. Though the period of 27.8 days is somewhat longer than the period of 27.4 days found in this study, the difference between the two period values may be caused by different time series adopted. Moreover, the global power spectra are the time-averaged wavelet spectrum of the local “components” of continuous wavelet power spectra over all time intervals considered, and thus the method can be used to identify dominant periods. Consequently, we infer that the accurate value of the most dominant rotation period in B_x , B_y , and B_z components is 27.4 days.

Various solar tracers that are located at different heights in the solar atmosphere, as well as various solar activity indicators that are also derived from the different layers of the solar atmosphere, were used to study the solar (differential) rotation, and the results indicated that the rotation periods of the different layers in the solar atmosphere are different from one another (Gilman & Howard 1984; Sheeley et al. 1992; Rybak 1994; Brajša et al. 2001, 2002; Altrock 2003; Song & Wang 2005; Javaraiah et al. 2005; Wöhl et al. 2010; Li et al. 2013; Shi & Xie 2014; Javaraiah & Bertello 2016; Xie et al. 2017b), though the rotation periods shown in these studies are very close to 27 days. The daily solar spectral irradiances in the

spectral ranges of 1–39 nm and 116–2416 nm that are derived from different heights in the solar atmosphere were used by Li et al. (2019) to investigate the solar rotation characteristics from the photosphere to the corona. The authors found that the rotation periods in coronal plasma and in the solar atmosphere at the bottom of the photosphere that is modulated by magnetic structures are 26.3 and 27.5 days, respectively. The 27.5-day rotation period in the photosphere is very consistent with the rotation period of 27.4 days in both the B_x and B_y components. Moreover, it is well known that the interplanetary magnetic flux consists of two components. One is the constant open-flux component that mainly originates from coronal holes, although some fraction of the open flux may be derived from an unknown source of quiet-Sun slow wind, and the other is a time-varying contribution that is closely related to the ejected associated flux carried by coronal mass ejections (e.g., McComas et al. 1992; Owens & Crooker 2006, 2007; Schwadron et al. 2010; Linker et al. 2017). Xiang & Qu (2018) further pointed out that the constant open-flux component in interplanetary magnetic flux probably originates mainly from the activity of the weak magnetic field activity on the solar disk, and the time-varying component in IMF is closely related to active regions (strong magnetic field activity) on the solar surface. The authors also suggested that the short-term periodicities of IMF intensity on the timescales of a few days to weeks are driven by magnetic activity on the solar surface. Consequently, it seems that the rotation period for both the B_x and B_y components is mainly due to the modulation of the joint effect of weak and strong magnetic activity in the solar photosphere. On the other hand, Echer & Svalgaard (2004) found that the rotation period of about 27 days in IMF polarity is modulated by the disturbance of the heliospheric current sheet. They implied that a more stable and flat heliospheric current sheet only appears in the ascending phase of solar cycles, which is strongly disturbed in the declining solar cycle phase by corotating interaction regions arising from the coronal hole high-speed streams overtaking the slow solar wind, and such disturbance of the heliospheric current sheet lasts during solar minimum. Moreover, the signals of rotation period for IMF B_x and B_y components in this study are almost the same as that for IMF polarity shown in Echer & Svalgaard (2004). Especially, both studies show that the 27-day signal is absent around the 1990s minimum. Thus, the disturbance of the heliospheric current sheet should also be a major factor to

modulate the rotation period for both B_x and B_y components around the declining phase and minimum time of solar cycles. For the B_z component, the rotation period of 27.4 days indicates that its rotation is also modulated by the solar magnetic activity in the solar photosphere. At the same time, the periodic behavior of the B_z component in GSM is influenced by the Russell–McPherron effect (Russell & McPherron 1973), and the rotation period for B_z shows a seasonal dependence, which is due to an exquisite harmony between the Russell–McPherron effect and the IMF sector structure that displays either two or four sectors for a long time interval (Choi & Lee 2019). Thus, the local wavelet power spectra of the B_z component are found to intermittently appear, which are different from those of the B_x and B_y components.

Based on the results of the wavelet analysis, we study the dependence of the rotation cycle lengths of the daily B_x , B_y , and B_z on the phase of the solar cycle relative to the nearest preceding sunspot minimum. Figures 3 and 4 show that the profile of rotation cycle lengths of the B_x component is almost the same as that of the B_y component. The rotation cycle lengths for the daily B_x and B_y vary with solar cycle phase. The statistical significance test shows that the variations between the maximum and minimum values of the rotation cycle lengths for the IMF B_x (B_y) component shown in Figure 4 are significant at the 95% confidence level. The profile of rotation cycle lengths can to some extent truly reflect the dependence of the rotation cycle lengths for the B_x (B_y) component on the solar cycle phase. As Figure 4 shows, the rotation cycle lengths in both the B_x and B_y components increase from the start to the first year of a new Schwabe cycle and then decrease gradually from the first to the fourth year of the Schwabe cycle. With the end of the former old solar cycle, and with a new Schwabe solar cycle beginning, more and more active regions that belong to the new Schwabe cycle can be found at high latitudes, indicating that these new emerging active regions have relatively low rotation rates. This is why the rotation cycle lengths of two time series increase from the start to the first year of a new Schwabe cycle. With the advance of solar cycle, the active regions gradually form at relatively low latitudes, and the rotation rate of these active regions should slightly increase. This can explain the gradual decrease of rotation cycle lengths in both the B_x and B_y components from the first to the fourth year of the Schwabe cycle. The profiles of temporal evolution of the rotation cycle lengths for both the IMF B_x and B_y components from the start to the fourth year of the Schwabe cycle are very similar to that for sunspot groups (Brajša et al. 2006) and the Mount Wilson Sunspot Index (Xiang et al. 2014) located in the corresponding time of the solar cycle. Thus, it is inferred that the variation of rotation cycle lengths for both the B_x and B_y components from the start to the fourth year of the Schwabe cycle is mainly due to the latitudinal migration and differential rotation feature of the activity regions, namely, it is mainly related to the strong magnetic activity in the photosphere. Figure 4 also shows that the rotation cycle lengths for both the B_x and B_y components fluctuate around the 27.4-day period within a small amplitude from the fourth year to the end of the Schwabe solar cycle. When solar activity occurs in this phase, solar activity regions mainly appear at relatively low latitudes with low migration velocity (Li et al. 2001a). Moreover, the rotation period for both the B_x and B_y components is also detected during the activity minima (Figures 2 and 3), showing that the variation of the rotation

cycle lengths is also modulated by the weak magnetic activity on the solar surface. Many studies reported that a higher average rotation velocity of sunspots can be clearly found in activity minima (Gilman & Howard 1984; Gupta et al. 1999; Khutsishvili et al. 2002; Brajša et al. 2006), and the rotation rate of small-scale magnetic structures is higher than that of large sunspots (Howard 1984; Xu & Gao 2016; Li et al. 2019). At the same time, the heliospheric current sheet is flat and calm in the ascending phase but is strongly disturbed in the declining phase because of the effect of corotating interaction regions arising from the coronal hole high-speed streams overtaking the slow solar wind, and such disturbance lasts during solar minimum (Echer & Svalgaard 2004). This should also be a major factor to modulate the rotation period for both the B_x and B_y components in this phase. Due to the joint effect of these activity regions located at relatively low latitudes (strong magnetic activity), weak magnetic activity (small-scale magnetic structures) on the solar surface, and the strong disturbance of the heliospheric current sheet, the rotation cycle lengths for both the B_x and B_y components show relatively low period values with small variation from the fourth year to the end of the Schwabe solar cycle. We also consider the dependence of the rotation cycle lengths for the corona on the solar cycle phase; however, the profile of temporal evolution of the rotation cycle lengths for the corona (Li et al. 2012; Xie et al. 2017b) is almost different from that for the B_x and B_y components. Such dependence of the rotation cycle lengths for both the B_x and B_y components on the solar cycle phase in turn indicates that the variation of the rotation period of the two time series is mainly modulated by the different physical origins around different solar cycle phases. For the B_z component, the dependence of the rotation cycle length for the B_z component on the solar cycle phase may not have the cycle-related variation.

Figure 6 shows the temporal variation of the rotation cycle lengths for both the B_x and B_y components, which is based on the local wavelet power spectra of the two time series. The results shown in this figure validate the aforementioned results: the longest rotation cycle length in each solar cycle always appears near 1 yr after the start of a new Schwabe solar cycle, and the shortest one seems to always occur near the solar maximum times. However, the longest and shortest rotation cycle lengths for the B_z component seem to appear in an arbitrary phase of solar cycles (Figure 5), and thus we cannot determine whether the rotation cycle lengths around the solar maximum time should be longer or shorter than those around the minimum time. We also use the method of autocorrelation analysis to study the periodicity in the temporal variation of the rotation cycle lengths for both the B_x and B_y components, and the results are shown in Figure 7. It is found that the significant periods for the 1 yr smoothed rotation periods of the B_x component are about 2.9, 3.4, 4.3, 4.9, 10.5, and 11.9 yr, and there exist significant periods of about 3.4, 9.9, and 14.1 yr in the 1 yr smoothed rotation periods of the B_y component. We do not study the periodicity in the temporal variation of B_z rotation, since the significant rotation cycle lengths for B_z appear intermittently during the entire time interval we considered, and there is no suitable mathematical method to make further analysis.

The periods in the range of 0.6–4 yr found in various solar activity indicators are often considered as QBOs, which should be derived from the base of the solar convection zone, and are

usually found from the base of the solar convection zone in the solar interior to the heliosphere (Bazilevskaya et al. 2000, 2014; Bumba 2003; Kane 2005; Vecchio et al. 2012; Xiang 2019). The periods of 2.9 and 3.4 yr found in the temporal variation of the B_x rotation and the period of 3.4 yr detected in the temporal variation of the B_y rotation are thus so-called QBOs. Early studies related to the temporal variation of solar rotation determined from different solar activity indicators showed similar periods (Javaraiah & Komm 1999; Javaraiah et al. 2009; Li et al. 2011; Xie et al. 2017b; Deng et al. 2020). For instance, several research groups found that the variation of the solar (differential) rotation based on analyzing sunspot data shows periods of about 2.1, 2.6, 3.1, and 3.9 yr (Javaraiah & Gokhale 1995; Javaraiah 1999; Li et al. 2011). The temporal variation of coronal rotation shows periods of about 2.1 and 3.0 yr determined from the daily 10.7 cm radio flux (Xie et al. 2017b), and that of about 3.25 yr obtained through analyzing the modified coronal index (Deng et al. 2020). Our analysis results further demonstrate the existence of QBOs in the temporal variation of the rotation cycle lengths for both the IMF B_x and B_y components. One should keep in mind that the interplanetary magnetic flux is rooted in the solar photosphere, and it consists of two components: the time-varying contribution that is closely related to the ejected associated flux carried by coronal mass ejections is related to active regions (strong magnetic field activity) on the solar surface, and the constant open-flux component that is mainly derived from coronal holes originates from the activity of the weak magnetic fields (e.g., Webb & Howard 1994; Owens et al. 2008; Smith et al. 2013; Xiang & Qu 2018). Moreover, Lockwood (2001) and Bazilevskaya et al. (2014) pointed out that the solar QBOs can be transmitted into interplanetary space by the open magnetic flux. Based on these results, we consider that the QBOs in the periodic variation of the rotation cycle lengths for both the IMF B_x and B_y components are related to the solar QBOs.

The periods of 4.3 and 4.9 yr exist in the temporal variation of B_x rotation, but they disappear in the temporal variation of the rotation cycle lengths of the B_y component. A similar 4.8 yr period was found by Javaraiah & Gokhale (1995) and Javaraiah (1999), respectively, in the periodic variation of solar differential rotation obtained through analyzing the time series of sunspot group and in the variation of solar rotation determined from Mount Wilson velocity data. Moreover, the temporal variation of the equatorial rotation rate of sunspot groups has a similar period of about 4.9 yr (Javaraiah & Bertello 2016); the rotation rate of large-scale magnetic field near the equator in the photosphere varies in time with a period in the range of 4.2–4.5 yr (Gavryuseva & Godoli 2006). Xie et al. (2018) also reported that the periods of 4.4 and 4.8 yr were found in the variation of the equatorial rotation rate determined from the solar magnetic fields. Our study further confirms the existence of about four to five periods in the temporal variation of rotation periods of the B_x component, which may be derived from the magnetic activity on the solar surface. On the other hand, one can see that several periods exist in the temporal variation of B_x rotation on timescales of 2–5 yr, but only the period of 3.4 yr on those timescales is found in the periodic variation of the rotation cycle lengths of the B_y component. The magnetic activity on the solar surface has more pronounced influence on the temporal variation of B_x rotation than that of B_y rotation on timescales of 2–5 yr.

The period of about 11 yr in the temporal variation of solar rotation determined from different solar activity indicators has been found by many researchers (Javaraiah 1999; Javaraiah & Komm 1999; Obridko & Shelting 2001; Li et al. 2013; Xie et al. 2017a, 2017b). However, the quasi-11 yr period in the variation of both B_x and B_y rotation has not been discussed so far. Our analysis shows a significant period of about 10.5 yr in the 1 yr smoothed rotation periods of the B_x component and a significant period of about 9.9 yr in the 1 yr smoothed rotation periods of the B_y component. Similarly, Javaraiah (1999) reported a period of about 9.6 yr in the variation of the solar rotation determined from Mount Wilson velocity data. Brajša et al. (2006) found a period of about 10.6 yr in the temporal variation of the solar rotation derived from sunspot groups. Li et al. (2013) and Xie et al. (2018) also suggested the existence of a 10.5 yr period in the variation of equatorial rotation rate of solar magnetic fields. In the corona, Xie et al. (2017b) and Deng et al. (2020) reported the existence of the quasi-11 yr period in the temporal variation of coronal rotation, which should be related to the 11 yr Schwabe solar cycle. The solar mean magnetic field reflects an integrated characteristic of the Sun, and the variation of the rotation periods of the solar mean magnetic field also has a significant period of about 10.1 yr (Xie et al. 2017a). From these early studies, one can know that the quasi-11 yr period can be found in the temporal variation of solar rotation determined from different indicators located in the solar atmosphere from the photosphere to the corona. The IMF originates from the solar magnetic field that is carried out by solar wind to the heliosphere. Thus, the periods of 10.5 and 9.9 yr found in this study prove that the quasi-11 yr period also exists in the temporal variation of both B_x and B_y rotation, which should be related to the 11 yr Schwabe solar cycle.

The phase relation between the rotation cycle lengths of the IMF B_x (B_y) and solar activity is analyzed by the method of cross-correlation analysis, and the result is shown in Figure 8. It shows that there exists a phase difference between the rotation cycle lengths of B_x (B_y) and solar activity, indicating that the relationship between rotation lengths of two time series and the solar activity is complex. Such a complex phase relation may be caused by the complex solar cycle phase dependence of the rotation cycle lengths of the IMF B_x (B_y) component, which is discussed in detail in the aforementioned results. Furthermore, our analysis also finds that the phase difference between the rotation cycle lengths of the B_x component and solar activity is different from that between rotation cycle lengths of the B_y component and solar activity. We do not further analyze the exact phase relationship among the three time series in this study, and it will be interesting to further study this topic in the future.

The autocorrelation analysis also indicates the existence of the period of 11.9 yr in the 1 yr smoothed rotation periods of the B_x component and the period of 14.1 yr in the 1 yr smoothed rotation periods of the B_y component, two of which seem to be longer than the 11 yr Schwabe solar cycle. It is well known that the solar activity cycle is not a strict 11 yr cycle, and the length of the solar cycle for a certain activity cycle is generally longer or shorter than 11 yr (Mendoza 1999; Brajša et al. 2006; Hathaway 2015). The period of 11.9 yr in the variation of B_x rotation may be related to the relatively longer solar activity cycle. However, the period of 14.1 yr in the variation of B_y rotation should link to other physical mechanisms. Generally, the solar cycle length is the time

interval of two successive sunspot minima. Actually, the former old solar activity cycle overlaps the subsequent new one by 2–3 yr, which is often referred to as the extended cycle of solar activity (Harvey 1992; Li et al. 2001b; Cliver 2014; Hathaway 2015). Sunspot activity regions that belong to the new Schwabe cycle emerge at high latitudes around its minimum time, but solar activity regions of the former old solar cycle still appear near the equator. Since there exist overlapping emergences of solar activity regions, the length of the extended cycle of solar activity is about 14–16 yr (Harvey 1992; Cliver 2014). We consider that the period of 14.1 yr in the variation of B_y rotation may be related to the extended cycle of solar activity.

Generally, the temporal variation of the rotation period for the B_x component is almost consistent with that for the B_y component, since the rotation period for the two time series is mainly derived from the modulation of the magnetic activity on the solar surface in the ascending phase, and should be due to the joint effect of the strong disturbance of the heliospheric current sheet and magnetic activity on the solar surface in the declining phase and minimum time of solar cycles. But for the B_z component, not only is the rotation period modulated by the solar magnetic activity, but also its periodic behavior is largely related to the structure of the coronal field polarity (Choi & Lee 2019). Thus, the temporal variation of the rotation period for the B_z component is totally different from that for the B_x and B_y components.

For the temporal evolution of intermittent periods other than the rotation period of about 27 days in the IMF B_x , B_y , and B_z components, the result of wavelet analysis shown in Figure 2 indicates that the significant periods of 9–16 days appear in the B_x , B_y , and B_z components, which peak at 13.7 days in B_x and B_y and 13.9 days in B_z , which should be the first solar rotation harmonics. However, the wavelet power spectra show that the significant variations of the three time series on this timescale appear intermittently during the entire time interval we considered except for that in the declining phases of solar cycles 21 and 22. Such intermittent appearance of the significant periods for the B_x , B_y , and B_z components makes it impossible to further analyze the temporal variation of the first solar rotation harmonics.

The periods of about 150–200 days detected in various solar activity indicators are referred to as “Rieger-type” periods (Rieger et al. 1984; Lou 2000; Knaack et al. 2005; Zaqarashvili et al. 2010; Gurgenchashvili et al. 2016; Xiang 2019, and references therein). On this timescale, the possible period of 184.3 days is detected in the B_x and B_z components, and the possible period of about 187.0 days is found in the B_y component. The global power spectra show that these periods are below the 95% confidence level, since the global power spectra are the time-averaged values of the local “components” of continuous wavelet power spectra over all time intervals considered (span of 52 yr), but the Rieger-type period is not always present in all solar cycles and usually appears in episodes of 1–3 yr (Lean 1990; Oliver et al. 1998; Krivova & Solanki 2002; Zaqarashvili et al. 2010). As the left panel of Figure 2 shows, the significant regions above the 95% confidence level for B_x on the timescales of Rieger-type periods only appear in the time interval of 1982–1984, which for B_y are intermittently found near 1971, 1983, 1989, and 2003, and that for B_z only appear in solar cycle 22. Hence, these periods found in B_x , B_y , and B_z should be Rieger-type

periods, which should be related to the Rieger-type periods of solar magnetic activity.

The QBOs are also found in the local wavelet power spectra of the B_x , B_y , and B_z that are displayed in the left panel of Figure 2. As this figure shows, the significant regions of above 95% confidence level in the range of 256–512 days (peak at 1.01 yr) for B_x intermittently appear during 1975–2000, and those in the range of 256–600 days (peak at 1.02 yr) for B_y are also intermittently found during 1975–2000. The QBOs for B_z only appear in solar cycle 22, which corresponds to the significant period of 0.90 yr, and also peak at 1.58 and 2.77 yr. The possible period of 3.45 yr for B_x does not show the corresponding significant region in the local wavelet power spectrum. The significant region that corresponds to the possible period of 2.37 yr for B_y appears near 1992. Early study proved that the solar QBOs can be transmitted into interplanetary space by the open magnetic flux (Lockwood 2001; Bazilevskaya et al. 2014); thus, the QBOs found in the B_x , B_y , and B_z components should be related to the solar QBOs. On the other hand, the annual variation in the IMF polarity in the band of 256–512 days, which is referred to the Rosenberg–Coleman effect (Rosenberg & Coleman 1969), only appears in the ascending phase of solar cycles by studying the IMF polarity date for the years 1927–2002 through the wavelet analysis method (Echer & Svalgaard 2004). The authors indicated that such a result should be attributed to a more stable and flat heliospheric current sheet that only appears in the ascending phase of solar cycles and strong disturbance of the heliospheric current sheet that is present in the declining phase and minimum time of solar cycles, and the Rosenberg–Coleman effect had been confirmed by the IMF B_x component during 1964–2002. The wavelet power spectra of the IMF B_x and B_y components in Figure 2 show that the annual variation in two time series can also be found in some, but not all, ascending phases of solar cycles, which is partly similar to the wavelet map of the IMF polarity in Echer & Svalgaard (2004). Thus, the annual variation in the IMF B_x and B_y components is also modulated by the stability or strong disturbance of the heliospheric current sheet. However, the wavelet power spectra of the IMF B_z show a different result, which indicates that the annual variation in this time series should not be related to the heliospheric current sheet.

The authors thank the anonymous referee for their careful reading of the manuscript and for constructive comments that improved the original version. We also express deep appreciation to the OMNI database of NASA and its staffs. This work is supported by the National Natural Science Foundation of China (grant Nos. 11633008 and 11603069), the Key Laboratory of Dark Matter and Space Astronomy, Project Supported by the Specialized Research Fund for State Key Laboratories, the Collaborating Research Program of CAS Key Laboratory of Solar Activity (KLSA201911), and the Chinese Academy of Sciences.

ORCID iDs

Z. J. Ning  <https://orcid.org/0000-0002-9893-4711>

References

- Altrock, R. C. 2003, *SoPh*, 213, 23
- Badruddin, & Kumar, A. 2015, *SoPh*, 290, 1271
- Bazilevskaya, G., Broomhall, A.-M., Elsworth, Y., & Nakariakov, V. M. 2014, *SSRv*, 186, 359

- Bazilevskaya, G. A., Krainev, M. B., Makhmutov, V. S., et al. 2000, *SoPh*, **197**, 157
- Brajša, R., Ruždjak, D., & Wöhl, H. 2006, *SoPh*, **237**, 365
- Brajša, R., Wöhl, H., Vršnak, B., et al. 2001, *A&A*, **374**, 309
- Brajša, R., Wöhl, H., Vršnak, B., et al. 2002, *A&A*, **392**, 329
- Bumba, V. 2003, in *Solar Variability as an Input to the Earth's Environment*, ed. A. Wilson (Noordwijk: ESA), 3
- Cane, H. V., Richardson, I. G., & von Roseninge, T. T. 1998, *GeoRL*, **25**, 4437
- Chandra, S., & Vats, H. O. 2011, *MNRAS*, **414**, 3158
- Chernosky, E. J., & Hagan, M. P. 1958, *JGR*, **63**, 775
- Choi, K.-E., & Lee, D.-Y. 2019, *SoPh*, **294**, 44
- Chowdhury, P., Choudhary, D. P., Gosain, S., et al. 2015, *Ap&SS*, **356**, 7
- Chowdhury, P., & Dwivedi, B. N. 2011, *SoPh*, **270**, 365
- Clover, E. W. 2014, *SSRv*, **186**, 169
- Cole, T. W. 1973, *SoPh*, **30**, 103
- Deng, L., Qi, Z., Dun, G., & Xu, C. 2013, *PASJ*, **65**, 11
- Deng, L. H., Xiang, Y. Y., Qu, Z. N., et al. 2016, *AJ*, **151**, 70
- Deng, L. H., Zhang, X. J., Deng, H., et al. 2020, *MNRAS*, **491**, 848
- Dungey, J. W. 1961, *PhRvL*, **6**, 47
- Echer, E., & Svalgaard, L. 2004, *GeoRL*, **31**, L12808
- Edelson, R. A., & Krolik, J. H. 1988, *ApJ*, **333**, 646
- Gao, P. X. 2016, *ApJ*, **830**, 140
- Gavryuseva, E., & Godoli, G. 2006, *PCE*, **31**, 68
- Gilman, P. A., & Howard, R. 1984, *ApJ*, **283**, 385
- Gonzalez, A. L. C., & Gonzalez, W. D. 1987, *JGR*, **92**, 4357
- Gonzalez, W. D., Joselyn, J. A., Kamide, Y., et al. 1994, *JGR*, **99**, 5771
- Gonzalez, W. D., & Mozer, F. S. 1974, *JGR*, **79**, 4186
- Gopalswamy, N., Yashiro, S., & Akiyama, S. 2007, *JGRA*, **112**, A06112
- Grinstead, A., Moore, J. C., & Jevrejeva, S. 2004, *NPGeo*, **11**, 561
- Gupta, S. S., Sivaraman, K. R., & Howard, R. F. 1999, *SoPh*, **188**, 225
- Gurgenshvili, E., Zaqarashvili, T. V., Kukhianidze, V., et al. 2016, *ApJ*, **826**, 55
- Harvey, K. L. 1992, *ASP Conf. Ser.* 27, *The Solar Cycle* (San Francisco, CA: ASP), 335
- Hathaway, D. H. 2015, *LRSP*, **12**, 4
- Hathaway, D. H., Wilson, R. M., & Reichmann, E. J. 1994, *SoPh*, **151**, 177
- Howard, R. 1984, *ARA&A*, **22**, 131
- Javaraiah, J. 1999, *BASI*, **27**, 73
- Javaraiah, J., & Bertello, L. 2016, *SoPh*, **291**, 3485
- Javaraiah, J., Bertello, L., & Ulrich, R. K. 2005, *ApJ*, **626**, 579
- Javaraiah, J., & Gokhale, M. H. 1995, *SoPh*, **158**, 173
- Javaraiah, J., & Komm, R. W. 1999, *SoPh*, **184**, 41
- Javaraiah, J., Ulrich, R. K., Bertello, L., et al. 2009, *SoPh*, **257**, 61
- Kane, R. P. 2005, *SoPh*, **227**, 155
- Katsavrias, C., Preka-Papadema, P., & Moussas, X. 2012, *SoPh*, **280**, 623
- Khutsishvili, E. V., Gigolashvili, M. S., & Kvernadze, T. M. 2002, *SoPh*, **206**, 219
- Knaack, R., Stenflo, J. O., & Berdyugina, S. V. 2005, *A&A*, **438**, 1067
- Krivova, N. A., & Solanki, S. K. 2002, *A&A*, **394**, 701
- Lean, J. 1990, *ApJ*, **363**, 718
- Li, K. J., Gao, P. X., & Zhan, L. S. 2009, *ApJ*, **691**, 537
- Li, K. J., Liang, H. F., Feng, W., et al. 2011, *Ap&SS*, **331**, 441
- Li, K. J., Shi, X. J., Feng, W., et al. 2012, *MNRAS*, **423**, 3584
- Li, K. J., Xie, J. L., & Shi, X. J. 2013, *ApJS*, **206**, 15
- Li, K. J., Xu, J. C., Yin, Z. Q., et al. 2019, *ApJ*, **875**, 90
- Li, K. J., Yun, H. S., & Gu, X. M. 2001a, *AJ*, **122**, 2115
- Li, K. J., Yun, H. S., & Gu, X. M. 2001b, *ApJL*, **554**, L115
- Linker, J. A., Caplan, R. M., Downs, C., et al. 2017, *ApJ*, **848**, 70
- Lockwood, M. 2001, *JGR*, **106**, 16021
- Lou, Y.-Q. 2000, *ApJ*, **540**, 1102
- McComas, D. J., Gosling, J. T., & Phillips, J. L. 1992, *JGR*, **97**, 171
- Mendoza, B. 1999, *SoPh*, **188**, 237
- Mursula, K., & Vilppola, J. H. 2004, *SoPh*, **221**, 337
- Neugebauer, M., Smith, E. J., Ruzmaikin, A., Feynman, J., & Vaughan, A. H. 2000, *JGR*, **105**, 2315
- Obridko, V. N., & Shelting, B. D. 2001, *SoPh*, **201**, 1
- Oliver, R., Ballester, J. L., & Baudin, F. 1998, *Natur*, **394**, 552
- Owens, M. J., & Crooker, N. U. 2006, *JGRA*, **111**, A10104
- Owens, M. J., & Crooker, N. U. 2007, *JGRA*, **112**, A06106
- Owens, M. J., Crooker, N. U., Schwadron, N. A., et al. 2008, *GeoRL*, **35**, L20108
- Prabhakaran Nayar, S. R., Radhika, V. N., Revathy, K., et al. 2002, *SoPh*, **208**, 359
- Pulkkinen, T. 2007, *LRSP*, **4**, 1
- Rieger, E., Share, G. H., Forrest, D. J., et al. 1984, *Natur*, **312**, 623
- Rosenberg, R. L., & Coleman, P. J. 1969, *JGR*, **74**, 5611
- Russell, C. T., & McPherron, R. L. 1973, *JGR*, **78**, 92
- Rybak, J. 1994, *SoPh*, **152**, 161
- Schwadron, N. A., Connick, D. E., & Smith, C. 2010, *ApJL*, **722**, L132
- Sheeley, N. R., Wang, Y.-M., & Nash, A. G. 1992, *ApJ*, **401**, 378
- Shi, X. J., & Xie, J. L. 2014, *AJ*, **148**, 101
- Singh, Y. P., & Badruddin 2019, *SoPh*, **294**, 27
- Singh, Y. P., Gautam, S., & Badruddin 2012, *JASTP*, **89**, 48
- Smith, C. W., Schwadron, N. A., & DeForest, C. E. 2013, *ApJ*, **775**, 59
- Song, W., & Wang, J. 2005, *ApJL*, **624**, L137
- Souza, A. M., Echer, E., Bolzan, M. J. A., & Hajra, R. 2016, *JASTP*, **149**, 81
- Takalo, J., & Mursula, K. 2002, *GeoRL*, **29**, 1317
- Torrence, C., & Compo, G. P. 1998, *BAMS*, **79**, 61
- Tsichla, M., Gerontidou, M., & Mavromichalaki, H. 2019, *SoPh*, **294**, 15
- Vats, H. O. 2012, *P&SS*, **63**, 158
- Vecchio, A., Laurenza, M., Meduri, D., Carbone, V., & Storini, M. 2012, *ApJ*, **749**, 27
- Webb, D. F., & Howard, R. A. 1994, *JGR*, **99**, 4201
- Wöhl, H., Brajša, R., Hanslmeier, A., et al. 2010, *A&A*, **520**, A29
- Xiang, N.-B. 2019, *RAA*, **19**, 131
- Xiang, N. B., & Qu, Z. N. 2018, *AJ*, **156**, 152
- Xiang, N. B., Qu, Z. N., & Zhai, Q. 2014, *AJ*, **148**, 12
- Xie, J., Shi, X., & Qu, Z. 2018, *ApJ*, **855**, 84
- Xie, J.-L., Shi, X.-J., & Xu, J.-C. 2012, *RAA*, **12**, 187
- Xie, J. L., Shi, X. J., & Xu, J. C. 2017a, *AJ*, **153**, 171
- Xie, J. L., Shi, X. J., & Zhang, J. 2017b, *ApJ*, **841**, 42
- Xu, J. C., & Gao, P. X. 2016, *ApJ*, **833**, 144
- Zaqarashvili, T. V., Carbonell, M., Oliver, R., & Ballester, J. L. 2010, *ApJ*, **709**, 749